Gene prediction

If there was a cDNA match, gene predictions (except in Fig. 3a; see below) were based on the annotation provided by the rice full-length cDNA consortium[19]. If not, the annotation used was from the corresponding sequence provider or the annotation of rice contigs (version 07232003) from the Institute of Genomic Research (TIGR) (http://www.tigr.org). In Fig. 3a, the open reading frame (ORF) inside the Pack-MULE was defined by ORFfinder (http://www.ncbi.nlm.nih.gov) on the basis of the corresponding cDNA sequence[19].

Expression analysis

The full-length cDNA data set was downloaded from http://cdna01.dna.affrc.go.jp/cDNA/ on 15 November 2003. A Pack-MULE is considered to have a cDNA match if, first, sequence similarity between the Pack-MULE and the cDNA is higher than 99.5% over the entire length of the cDNA and, second, the chromosomal position of the Pack-MULE is consistent with the genomic position of the particular cDNA provided by the rice full-length cDNA consortium[19]. Peptide sequences representing 2,528 unique proteins were downloaded from ref. 20 (http://www.pnas.org) and used as queries to search against all Pack-MULE sequences recovered in both the genome-wide search and the search of chromosomes 1 and 10 with TBLASTN[20]. Peptide sequences that generated perfect hits with Pack-MULE sequences were then used to search the rice genomic database. A particular Pack-MULE sequence was considered to have a peptide match if it was the only perfect hit in the genome.

K_a/K_s analysis

The sequences of each Pack-MULE and its corresponding genomic homologue were aligned using the 'pileup' program from the University of Wisconsin GCG program suite (version 10.1) accessed through Research Computing Resources at the University of Georgia. The alignment was based on the ORF of the genomic homologue (see Supplementary Tables 6 and 10 for details). If the genomic homologue was not predicted as a coding sequence, the ORF of the MULE was used. K_a and K_s were calculated with MEGA using the Pamilo–Bianchi–Li method[24]. The significance of purifying selection (P value) was evaluated with the z-test in MEGA.

1. Lisch, D. *Mutator* transposons. *Trends Plant Sci.* **7**, 498–504 (2002).
2. Walbot, V. & Rudenko, G. N. in *Mobile DNA II* (eds Craig, N. L., Craigie, R., Gellert, M. & Lambowitz, A. M.) 533–564 (American Society of Microbiology Press, Washington, D.C., 2002).
3. Chalvet, F., Grimaldi, C., Kaper, F., Langin, T. & Daboussi, M. J. *Hop*, an active *Mutator*-like element in the genome of the fungus *Fusarium oxysporum*. *Mol. Biol. Evol.* **20**, 1362–1375 (2003).
4. Talbert, L. E. & Chandler, V. L. Characterization of a highly conserved sequence related to *mutator* transposable elements in maize. *Mol. Biol. Evol.* **5**, 519–529 (1988).
5. Yu, Z., Wright, S. I. & Bureau, T. E. *Mutator*-like elements in *Arabidopsis thaliana*. Structure, diversity and evolution. *Genetics* **156**, 2019–2031 (2000).
6. Turcotte, K., Srinivasan, S. & Bureau, T. Survey of transposable elements from rice genomic sequences. *Plant J.* **25**, 169–179 (2001).
7. Bennetzen, J. L. & Springer, P. S. The generation of *mutator* transposable element subfamilies in maize. *Theor. Appl. Genet.* **87**, 657–667 (1994).
8. Goff, S. A. *et al.* A draft sequence of the rice genome (*Oryza sativa* L. ssp. *japonica*). *Science* **296**, 92–100 (2002).
9. Normile, D. & Pennisi, E. The rice genome. Rice: boiled down to bare essentials. *Science* **296**, 32–36 (2002).
10. Yu, J. *et al.* A draft sequence of the rice genome (*Oryza sativa* L. ssp. *indica*). *Science* **296**, 79–92 (2002).
11. Bao, Z. & Eddy, S. R. Automated *de novo* identification of repeat sequence families in sequenced genomes. *Genome Res.* **12**, 1269–1276 (2002).
12. Cresse, A. D., Hulbert, S. H., Brown, W. E., Lucas, J. R. & Bennetzen, J. L. *Mu1*-related transposable elements of maize preferentially insert into low copy number DNA. *Genetics* **140**, 315–324 (1995).
13. Hanley, S. *et al.* Identification of transposon-tagged genes by the random sequencing of *Mutator*-tagged DNA fragments from *Zea mays*. *Plant J.* **23**, 557–566 (2000).
14. Le, Q. H., Wright, S., Yu, Z. & Bureau, T. Transposon diversity in *Arabidopsis thaliana*. *Proc. Natl Acad. Sci. USA* **97**, 7376–7381 (2000).
15. Taylor, L. P. & Walbot, V. A deletion adjacent to the maize transposable element *Mu-1* accompanies loss of *Adh 1* expression. *EMBO J.* **4**, 369–376 (1985).
16. Levy, A. A. & Walbot, V. Molecular analysis of the loss of somatic instability in the *bz2-mu1* allele of maize. *Mol. Gen. Genet.* **229**, 147–151 (1991).
17. Sasaki, T. *et al.* The genome sequence and structure of rice chromosome 1. *Nature* **420**, 312–316 (2002).
18. The Rice Chromosome 10 Sequencing Consortium. In-depth view of structure, activity, and evolution of rice chromosome 10. *Science* **300**, 1566–1599 (2003).
19. Kikuchi, S. *et al.* Collection, mapping, and annotation of over 28,000 cDNA clones from *japonica* rice. *Science* **301**, 376–379 (2003).
20. Koller, A. *et al.* Proteomic survey of metabolic pathways in rice. *Proc. Natl Acad. Sci. USA* **99**, 11969–11974 (2002).
21. Moran, J. V., DeBerardinis, R. J. & Kazazian, H. H. Jr. Exon shuffling by L1 retrotransposition. *Science* **283**, 1530–1534 (1999).
22. Emerson, J. J., Kaessmann, H., Betran, E. & Long, M. Extensive gene traffic on the mammalian X chromosome. *Science* **303**, 537–540 (2004).
23. Jiang, N. *et al.* An active DNA transposon in rice. *Nature* **421**, 163–167 (2003).
24. Kumar, S., Tamura, K., Jakobsen, I. B. & Nei, M. *MEGA2: Molecular Evolutionary Genetics Analysis software* (Arizona State Univ., Tempe, Arizona, 2001).

···

Small modulation of ongoing cortical dynamics by sensory input during natural vision

József Fiser[1,3], Chiayu Chiu[2] & Michael Weliky[1,3]

[1]Center for Visual Science, [2]Interdepartmental Program in Neuroscience, and [3]Department of Brain and Cognitive Sciences, University of Rochester, Rochester, New York 14627, USA

During vision, it is believed that neural activity in the primary visual cortex is predominantly driven by sensory input from the environment. However, visual cortical neurons respond to repeated presentations of the same stimulus with a high degree of variability[1–4]. Although this variability has been considered to be noise owing to random spontaneous activity within the cortex[5–7], recent studies show that spontaneous activity has a highly coherent spatio-temporal structure[8–13]. This raises the possibility that the pattern of this spontaneous activity may shape neural responses during natural viewing conditions to a larger extent than previously thought. Here, we examine the relationship between spontaneous activity and the response of primary visual cortical neurons to dynamic natural-scene and random-noise film images in awake, freely viewing ferrets from the time of eye opening to maturity. The correspondence between evoked neural activity and the structure of the input signal was weak in young animals, but systematically improved with age. This improvement was linked to a shift in the dynamics of spontaneous activity. At all ages including the mature animal, correlations in spontaneous neural firing were only slightly modified by visual stimulation, irrespective of the sensory input. These results suggest that in both the developing and mature visual cortex, sensory evoked neural activity represents the modulation and triggering of ongoing circuit dynamics by input signals, rather than directly reflecting the structure of the input signal itself.

Using an implanted multi-electrode array, we measured population activity within the visual cortex of awake, freely viewing ferrets at three different developmental stages: immediately after eye opening at postnatal day (P) 30–32 ($n = 3$), immediately after the maturation of orientation tuning and long-range horizontal connections at P44–45 ($n = 3$), and in the mature animal at P83–90 ($n = 4$). A linear array of 16 microwire electrodes, spanning 9.0 mm, was placed at 300–500-μm depth in layer 2/3 of the striate cortex, which allowed recordings to be obtained from cortical sites with varying degrees of receptive field overlap (Fig. 1a). Fifteen 100-s recording trials were acquired in head-restrained ferrets under each of three interleaved conditions: (1) presentation of dynamic natural scenes from a film; (2) presentation of dynamic random-noise stimuli; and (3) complete darkness (see Methods). At all ages,

both natural-scene and random-noise visual stimulation increased the mean and variance of neuronal firing rates as well as the percentage of active bins (that is, bins containing at least one spike) when compared with the same measures in the dark (Fig. 1b). Thus, both types of stimuli were able to drive neurons within the visual cortex.

Using a statistical approach in which the input signal and output neural responses were characterized by measuring their ensemble properties, we assessed the degree to which the activity of visual cortical neurons accurately reflects the spatio-temporal structure of the visual input. This was accomplished by computing temporal and spatial correlation functions for the dynamic natural-scene and random-noise stimuli, and comparing these with the same measures computed from neural activity recorded under the three experimental viewing conditions. Whereas correlation functions for the neural responses were computed from recorded multi-unit activity, those calculated for the dynamic natural-scene and random-noise stimuli were based on the response of a bank of linear filters applied to the two types of stimuli (see Methods). Such linear filters characterize the response properties of primary visual cortical neurons, which are strongly activated by changing high-contrast features, such as moving edges and junctions, and very weakly activated by low-contrast homogeneous image regions. Thus, the temporal and spatial correlation functions computed from these filter responses provide a statistical measure of the expected activation of neurons at different recording sites by image features in the dynamic stimulus displays.

As expected, the correlation functions computed from filter responses to dynamic random-noise and natural-scene stimuli were very different, demonstrating the diverse statistical properties of the two displays (Fig. 1c). The temporal correlation function for natural scenes revealed strong correlations extending to several hundred milliseconds, reflecting the continuity of images across successive film frames. On the other hand, filter responses to random noise were decorrelated at 30 Hz, consistent with random changes across consecutive frames in the stimuli. The spatial correlation function for random noise revealed a gradual decrease in correlated activity as a function of increasing distance between recording sites, reaching zero between sites whose receptive fields did not overlap. For natural scenes, high correlations were present between all recording sites irrespective of the distance between sites, due to the extended contours of objects that span non-overlapping receptive fields.

If neural activity evoked by visual stimulation was directly related to the input signal, then the different statistical properties of natural-scene and random-noise displays would be expected to trigger different patterns of neuronal firing within the primary visual cortex. To quantify the degree of similarity between
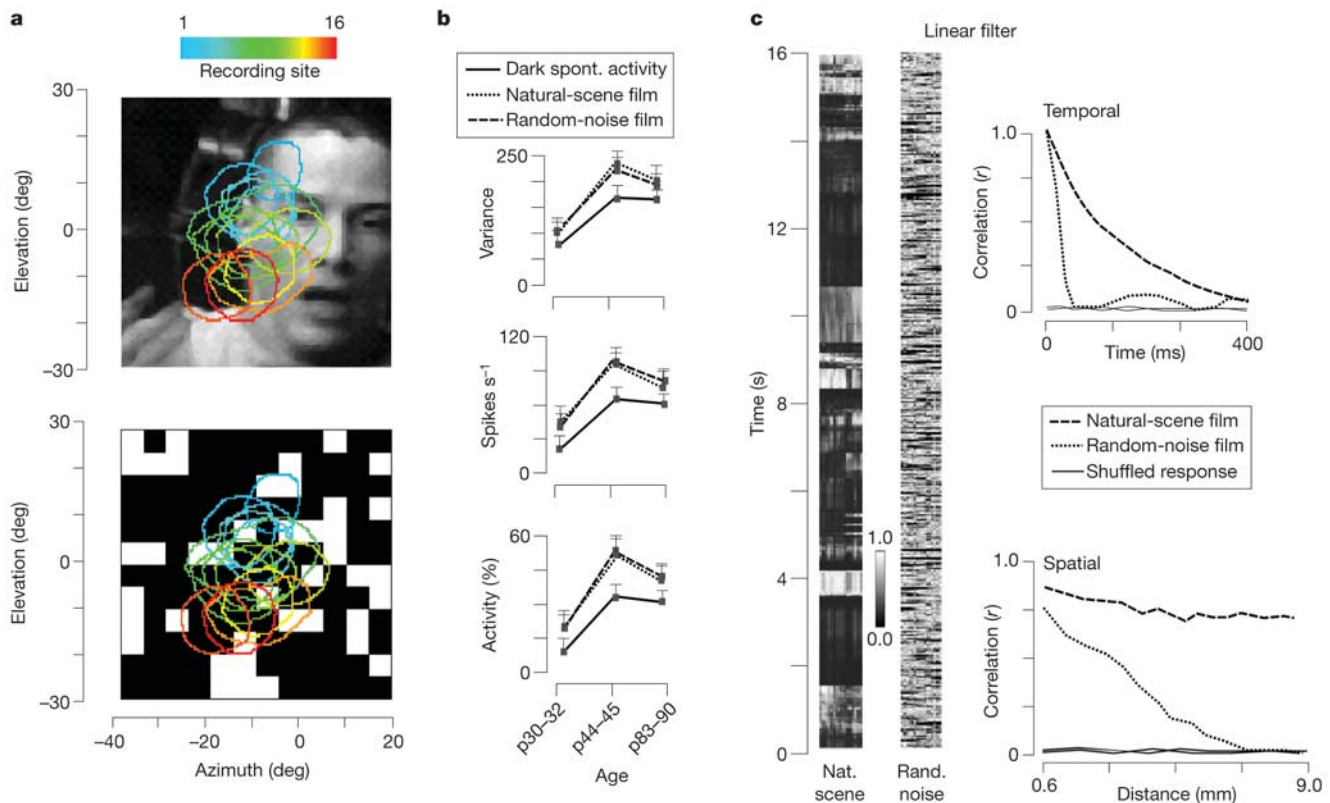

Figure 1 Statistical properties of natural-scene and random-noise film images.
a, Representative images from natural-scene film (top) and random-noise stimuli (bottom). The circles overlaid upon each image show mapped classical receptive fields for each of the 16 recording sites in a P83 ferret. Colour is used to distinguish the relative locations of receptive fields recorded at the different recording sites. The receptive fields for recording sites 1–3 and 14–16 are completely non-overlapping. A similar distribution of overlapping receptive fields was obtained in all younger P30–32 and P44–45 visual cortices. **b**, The variance of neuronal firing in spikes s^{-2} (top), the firing rate of neurons (middle), and the percentage of active spike bins (bottom) under the different stimulus conditions at all developmental ages. Bin width, 25 ms. Error bars represent s.e.m. **c**, Response of 16 linear filters to natural-scene and random-noise film images.

Orientation and spatial frequency tuning, as well as receptive fields and the impulse response functions of linear filters were derived from recordings obtained in a P45 ferret. Similar results were obtained from ferrets at all other developmental ages. Left: time series plots of linear filter responses to stimulus films. Columns represent the simulated activity of each of the 16 recording sites. In response to the natural-scene film, periods of strong activity (white), reflecting movement of high-contrast edges through the receptive fields, are separated by periods of weak activity (black), when no stimulus features drive the filters. Random-noise film images stimulate the filters more uniformly. Right: temporal and spatial correlation functions of filter responses for natural-scene and random-noise film images. Shuffled response refers to the control condition of randomized filter responses.

correlation functions computed for neural activity during the different viewing conditions, a linear regression coefficient was fitted to an initial segment of each correlation function (temporal correlation function, 50–200 ms; spatial correlation function, 0.6–3.0 mm). At P30–32, visual cortical neurons burst in a slow and irregular manner in the absence of and during visual stimulation (Fig. 2). As a result, identical temporal correlations extending to several hundred milliseconds and identical patterns of locally correlated activity between neighbouring cortical sites were observed under all three viewing conditions ($P > 0.05$, ANOVA) (Fig. 3a). During subsequent development, temporal correlations shortened while spatial correlations broadened for all viewing conditions. At P44–45, spatial correlation functions of neural activity during all three viewing conditions were still identical ($P > 0.05$, t-test). However, small differences in temporal correlations emerged between P30–32 and P44–45. Whereas temporal correlations in dark spontaneous activity and random-noise responses remained indistinguishable at P44–45 ($P > 0.05$, t-test), temporal correlations in natural-scene responses fell off at a slightly slower rate ($P < 0.05$, t-test).

With continued maturation of the visual cortex, spontaneous and visually evoked activity evolved to dominant synchronized oscillations by P83–90 (Figs 2 and 3b). Between P44–45 and P83–90, dark spontaneous activity and random-noise responses became increasingly temporally decorrelated (Fig. 3a), and temporal correlation functions under these two conditions remained indistinguishable ($P > 0.05$, t-test). Temporal correlations in natural-scene responses also became increasingly decorrelated between P44–45

and P83–90, but continued to be significantly different from the other two conditions ($P < 0.05$, t-test). As a result of these developmental shifts, temporal correlations in neural responses at P83–90 reflected the different statistical properties of the two stimuli: temporal correlations in natural-scene responses fell off at a slower rate than those of random-noise responses, which were rapidly decorrelated. The shift in neuronal firing patterns also led to changes in the spatial correlation functions. At P83–90, short- and long-range spatial correlations under all viewing conditions reached high levels that were nearly uniform between cortical sites regardless of their separation. The slopes of spatial correlation functions under dark and natural-scene viewing conditions were not significantly different ($P > 0.05$, t-test), and correlated activity was only 20% higher during viewing of natural scenes than in the dark. Notably, there was a significant difference between spatially correlated neural activity evoked by the two types of visual stimuli. For neighbouring cortical sites with overlapping receptive fields, correlations in neural activity during random-noise and natural-scene stimulation were equally high ($P > 0.05$, t-test). However, as the separation between cortical sites increased, the level of correlated activity fell off more steeply during random-noise viewing than during natural-scene viewing ($P < 0.05$, t-test). This difference in slope reflected the different spatial properties of the two stimuli: long-range correlations in natural scenes are significantly higher than those in random noise. These results demonstrate that, as a result of developmental shifts in spatial and temporal correlation functions, there was a significantly improved correspondence between visually evoked neural activity and the structure of the input signal with increasing age.

It is important to emphasize that even in the mature visual cortex, visually evoked changes in the rate and pattern of neural firing were much smaller than expected if neurons were primarily driven by sensory input. Although visual stimulation increased neural activity in the cortex, the firing rates of neurons during visual presentation increased by only 23% compared with those in the dark. At 50 ms, the difference in temporal correlation coefficients of natural-scene and random-noise displays was 0.47, as measured by the linear filter model, whereas the actual difference in evoked neural activity to the two stimuli was only 0.039 ± 0.008. Furthermore, spatial correlations evoked by random-noise stimuli did not fall off to zero at large cortical separations as predicted by the linear filter responses. Rather, the correlation coefficient dropped by only 20% to the mean level of spatial correlations present in ongoing activity. These modest changes were not merely due to averaging, as demonstrated by individual assessment of mean correlations in neuronal firing between each pair of recording sites (see Supplementary Information). At all ages, such pairwise analysis generated correlation patterns that were nearly identical under the different viewing conditions ($P > 0.05$, ANOVA). Taken together, these findings suggest that during natural viewing, spatio-temporal correlations in neural firing are not primarily governed by the statistical properties of the input signal, but rather are dominated by the correlational structure of ongoing activity.

Eye movements, or lack of visual stimulation, could be a potential cause of the reduced correspondence between evoked neural responses and the input statistics. To test this possibility, we monitored eye movements during random-noise and natural-scene presentation. Temporal and spatial correlations, re-computed after excluding portions of binned spike traces recorded when the eyes were closed or during saccadic eye-movements, were not significantly different from correlation functions computed using the full spike traces ($P > 0.05$, t-test) (see Supplementary Information). Thus, eye movement artefacts or inadequate visual stimulation cannot explain the relatively small modulation of spontaneous activity by the visual input.

The prolonged neuronal bursting observed in younger animals, which was responsible for the strong temporal correlations at these
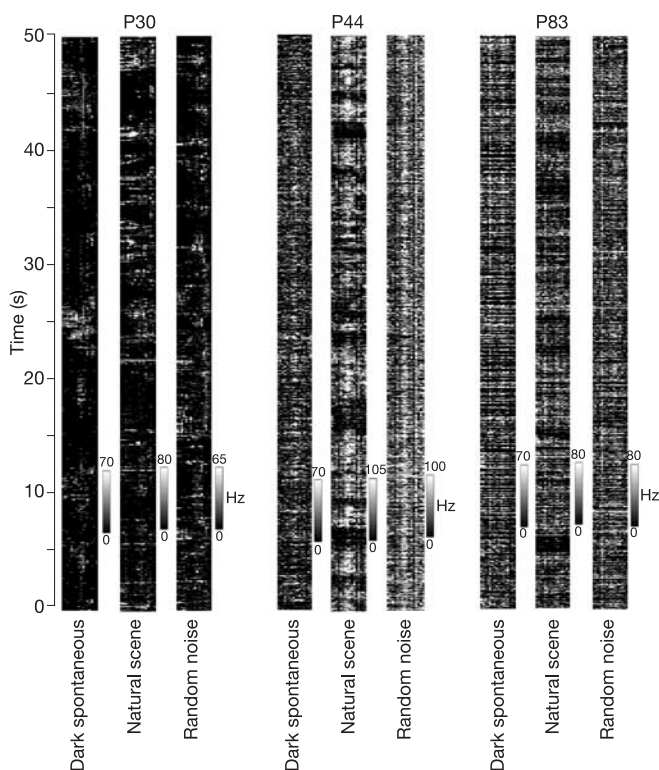

Figure 2 Time series plots of neural activity recorded under the three interleaved stimulus conditions at three different ages. The time series graphs were obtained from a single animal in each age group. At each age, visual stimulation modulates the spatio-temporal pattern of spontaneous activity, but does not significantly alter its basic correlational structure. At P44 and P83, the continuous spontaneous activity present across all recording sites is modulated during specific periods by the natural-scene film, presumably when a high-contrast feature moves across the receptive fields. The random-noise film image does not induce such significant modulations in firing rate. Bin width, 20 ms.
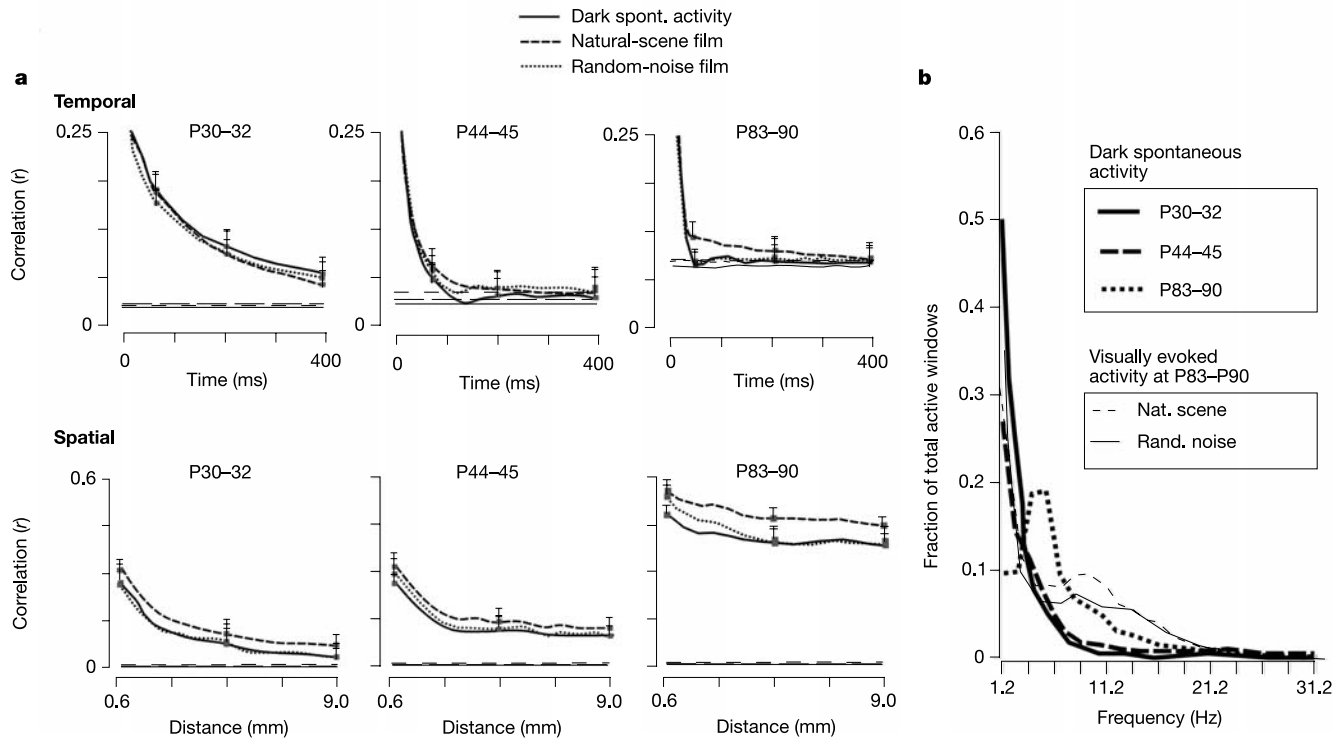
Figure 3 Developmental changes in the spatio-temporal pattern of stimulus-evoked and spontaneous visual cortical activity in awake-behaving ferrets. **a**, Correlation functions computed for dark spontaneous activity, as well as evoked activity to natural-scene and random-noise films in awake ferrets at three different ages. Thin horizontal lines show plots of correlation functions computed at each age for each condition using randomly shuffled binned spikes. Random temporal shuffling of spike trains abolished all correlations in all three age groups, demonstrating that the observed shifts in correlated activity were not simply a result of the developmental increase in cell firing rates. Top row: temporal correlation functions. Bin width, 20 ms. Bottom row: spatial correlation functions. Bin width, 50 ms. Error bars represent s.e.m. **b**, Emergence of oscillations in dark spontaneous activity during visual cortical development. Dominant 4–8-Hz oscillations emerge between P44–45 and P83–90. At P83–90, visual stimulation abolishes oscillations at these frequencies but triggers higher frequency oscillations. Total active windows are the total number of 800-ms windows that contained at least 1 spike.

ages, could be caused by either an intrinsic inability of neurons in the immature visual cortex to respond rapidly to visual stimuli, or by reverberating neural activity within immature feedback circuits[14]. To distinguish between these two possibilities, recordings were obtained from each animal under light anaesthesia using the same visual stimulation conditions as in the awake-behaving context (Fig. 4a). Light anaesthesia significantly dampened neuronal excitability, as demonstrated by a reduction in spontaneous activity, whereas neuronal responsiveness to visual stimulation was maintained (see Supplementary Information). In contrast to awake animals, temporal correlations, both during and in the absence of visual stimulation, showed swift decorrelation by 50 ms at all ages, including the youngest P30 animals (Fig. 4b, top). Thus, the slope of temporal correlation functions, computed for neural activity between 50–200 ms under all three stimulus conditions, was significantly reduced at P30–32 and P44–45 ($P < 0.05$, t-test) to levels matching those for control P83–90 animals (see Supplementary Information). This indicates that cortical neurons are capable of rapidly responding to sensory signals at all ages, and suggests that temporal correlations extending to several hundred milliseconds in the young awake animals may result from recurring activity generated within immature feedback circuits. In contrast, the spatial correlation functions were not substantially different for the awake and anaesthetized animal at any age (compare Fig. 4b, bottom, with Fig. 3a, bottom, $P > 0.05$, t-test). This suggests that feed-forward sensory evoked activity, which is maintained during anaesthesia, has a prominent role in governing the correlated firing of neurons between different cortical sites.

The strong correspondence between patterns of correlated

neuronal activity during and in the absence of visual stimulation, indicates a tight relationship between spontaneous activity and the cortical representation of sensory signals. Even when stimulated by input signals with diverse statistical properties, the firing patterns of visual cortical neurons are dominated by the intrinsic dynamical properties of the cortical circuit rather than the signal statistics. These results agree with previous reports in anaesthetized preparations and *in vitro* brain slices demonstrating that sensory evoked responses are significantly modulated by ongoing spontaneous neuronal activity, and that this spontaneous activity reflects the intrinsic dynamical behaviour of neural circuits[13,15–17]. They also agree with previous studies in nonhuman primates showing that the firing rates of visual cortical neurons are modulated to a smaller degree during free viewing of natural scenes than when the same stimuli are statically flashed within the classical receptive field during fixation[18,19]. However, our results are the first to demonstrate that intrinsic circuit dynamics strongly govern the correlated firing of neurons in primary visual cortex of freely viewing animals. These results provide the most direct evidence that the intrinsic dynamical behaviour of neural circuits might have a prominent role in visual sensory coding. If the specific spatio-temporal structure of these dynamics is important for normal sensory processing, then the shift from slow asynchronous bursting at early ages to dominant synchronous 4–8-Hz oscillations in the adult probably has a central role in the emergence of sensory coding during brain development.

Our analysis has focused only on second-order spatio-temporal correlations in spontaneous and visually driven activity, and it does not address higher-order correlations in neural activity that may also be used to encode input signals[20–22]. In addition, our results are

based on recording in the upper layers of the primary visual cortex. It is conceivable that cell responses in layer 4 are more readily related to the structure of the input stimulus[15,23,24]. Because of the high-energy consumption of baseline neural activity in the brain[25,26], it would be inefficient to maintain the observed high level of spon-

taneous activity unless it had an essential role in sensory processing. We propose that during sensory coding, stimulus-evoked activity in the visual cortex principally reflects the modulation and triggering of intrinsic circuit dynamical behaviour by sensory signals, instead of directly encoding the structure of the input signal itself. In this framework, ongoing activity may not be noise upon which visual responses are superimposed, but rather an integral component of sensory processing. □
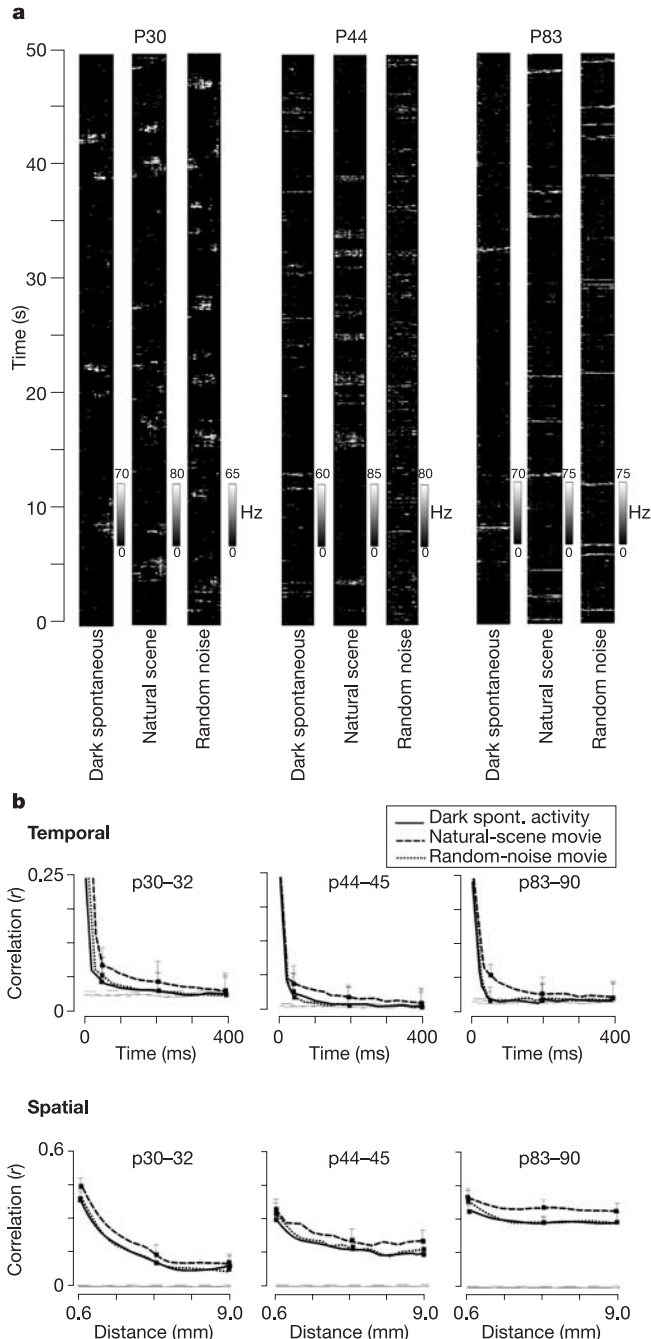
Methods

Electrode implant procedure

Surgical procedures were identical to those described previously[12]. Briefly, anaesthesia was induced and maintained during surgery by inhalation of isoflurane (0.5–2.0%) in a 2:1 nitrous oxide/oxygen mixture. A section of skull was exposed over area 17, the dura was reflected and the electrode array aligned along the caudal bank of the posterior lateral gyrus. After lowering the electrode array so that it touched the cortical surface, the exposed brain was covered by agar, and a headset was affixed by dental acrylic to the skull. A separate headpost holder was attached to the frontomedial skull by stainless steel screws and dental acrylic. All procedures were approved by the University of Rochester Committee on Animal Research.

Recording and data acquisition

The multi-electrode array consisted of a single row of 16 electrodes spaced at 600 µm (9.0-mm wide). Each electrode was a 12.5-µm-diameter tungsten wire with 2.5-µm H-ML insulation (California Fine Wire). The insulation along the final 30–60-µm length of wire was removed, creating a 200–300 kΩ impedance electrode. The electrodes typically provided clear multi-unit signal on each channel with occasional single unit signal. The average noise amplitude was 5.1 ± 0.9 µV, whereas the average signal amplitude was 34.4 ± 9.8 µV. All electrodes were simultaneously raised or lowered by turning a single, 100-thread-per-inch screw, and they were connected to custom-made amplifiers providing a gain of 20,000. The signal was band-pass-filtered between 600 and 6,000 Hz and digitized at 10,000 kHz via an AD board (National Instruments) to a PC. Data acquisition was performed with custom-written Labview programs (National Instruments). Spike discrimination was done offline by manually setting a separate voltage threshold for each electrode. Stable recordings were maintained for 8–12 h.

Recordings were initiated after 2–3 h of recovery from anaesthesia, when the animal was fully alert. There were delays of approximately 10–20 s between interleaved trials. After awake recordings, the same sessions were repeated under light anaesthesia (0.5–1.0% isoflurane in a 2:1 nitrous oxide/oxygen mixture) and then the receptive field properties were measured. Heart rate was monitored and body temperature was maintained with a thermostatically controlled heating blanket. At each of 16 recording sites, the position and size of receptive fields were determined by a reverse correlation method using an array of flashed white squares 2–3° on each side, and orientation and spatial frequency tuning were assessed by flashed high-contrast sine-wave gratings[27]. Stimuli were repeated at least eight times and evoked responses were averaged to obtain the receptive field structure and the temporal impulse response function. Drifting of receptive field positions across epochs was rarely encountered, and those epochs with receptive centres more than one square deviating from the mean were excluded from the analysis. Similar to earlier results, the receptive field sizes varied between 10–18° in size and were in the central 30° of the visual field at all three ages.

Visual stimulation

While the animal rested comfortably on a padded platform, the head was held in a fixed position with the use of a rigid metal post. The animal was free to make natural eye movements. A 4 × 3 foot stimulus screen, which was placed at a distance of 30 cm from the head, covered 130° by 100° visual angle. An LCD projector provided both random-noise and natural-scene stimuli, which covered the entire screen, at a resolution of 1,024 × 768 pixels and a refresh rate of 75 Hz. Random-noise stimuli were generated by a two-dimensional array of white squares, which were randomly flashed on a black background. For each frame, a square could appear with 25% uniform probability at each position in space, which occupied 5° × 5° visual angle. A new display was presented at a rate of 75 Hz. The trailer for the film *The Matrix* was used as the natural-scene film stimulus, which was presented at 24 Hz update rate and 720 × 480 resolution.

Correlation analysis

The temporal correlation function describes the mean correlation between spike firing rates measured at all recording sites at one particular time point, and successive time points. Discriminated spikes were placed into 20-ms bins. The Pearson product-moment correlation coefficient (r) was computed between population spike activity at each time bin t and successive time bins $t + n$. A histogram of the r-values at each $t + n$ interval was constructed across all time bins and all trials for each animal. The spatial correlation function describes the mean correlation r between the firing rates measured simultaneously at pairs of recording sites, parameterized by the distance between the recording sites.

Linear filter model

The spatial receptive fields of the linear filter model were constructed according to previously described procedures[27]. Briefly, the spatial properties of the filters were defined by experimentally measured receptive field size, shape and position, as well as the

Figure 4 Developmental changes in the spatio-temporal pattern of stimulus-evoked and spontaneous visual cortical activity in anaesthetized ferrets. **a**, Comparison of time series plots for dark spontaneous activity, natural-scene and random-noise films at three different ages. Plots are from a single animal at each age under the same stimulus conditions as awake animals. Bin width, 20 ms. **b**, Correlation functions computed for dark spontaneous activity, as well as evoked activity to natural-scene and random-noise film images in anaesthetized ferrets. Thin horizontal lines show plots of correlation functions computed at each age, using randomly shuffled binned spikes. Top row: temporal correlation functions. Bin width, 20 ms. Bottom row: spatial correlation functions. Bin width, 50 ms. Error bars represent s.e.m.

orientation and spatial frequency tuning, at each recording site for each animal. The temporal impulse functions were derived by generating a histogram of the neural responses to briefly presented flashes at random positions within the receptive field. Identical results were obtained with filters defined by parameters that were based on data obtained at each of the three age groups. The shapes of the correlational functions were relatively insensitive to the particular parameter values of the spatial and temporal filters.

Oscillation analysis

Oscillation frequency was computed separately at each recording site. First, discriminated spikes were placed into 2-ms bins. 800-ms windows of binned spikes were extracted every 200 ms, and the autocorrelation of the windowed spikes was computed, followed by the fast Fourier transform (FFT). The frequency with the maximum amplitude was determined, and a histogram of these frequencies was constructed.

1. Henry, G. H., Bishop, P. O., Tupper, R. M. & Dreher, B. Orientation specificity and response variability of cells in striate cortex. *Vision Res.* **13**, 1771–1779 (1973).
2. Schiller, P. H., Finlay, B. L. & Volman, S. F. Short-term response variability of monkey striate neurons. *Brain Res.* **105**, 347–349 (1976).
3. Vogels, R., Spileers, W. & Orban, G. A. The response variability of striate cortical neurons in the behaving monkey. *Exp. Brain Res.* **77**, 432–436 (1989).
4. Azouz, R. & Gray, C. M. Cellular mechanisms contributing to response variability of cortical neurons in vivo. *J. Neurosci.* **19**, 2209–2223 (1999).
5. Zohary, E., Shadlen, M. N. & Newsome, W. T. Correlated neuronal discharge rate and its implications for psychophysical performance. *Nature* **370**, 140–143 (1994).
6. Shadlen, M. N. & Newsome, W. T. The variable discharge of cortical neurons: Implications for connectivity, computation, and information coding. *J. Neurosci.* **18**, 3870–3896 (1998).
7. Pouget, A., Dayan, P. & Zemel, R. Inference and computation with population codes. *Annu. Rev. Neurosci.* **26**, 381–410 (2004).
8. Meister, M., Wong, R. O. L., Baylor, D. A. & Shatz, C. J. Synchronous bursts of action potentials in ganglion cells of the developing mammalian retina. *Science* **252**, 939–943 (1991).
9. Arieli, A., Shoham, D., Hildesheim, R. & Grinvald, A. Coherent spatiotemporal patterns of ongoing activity revealed by real-time optical imaging coupled with single-unit recording in the cat visual cortex. *J. Neurophysiol.* **73**, 2072–2093 (1995).
10. Weliky, M. & Katz, L. C. Correlational structure of spontaneous neuronal activity in the developing lateral geniculate nucleus in vivo. *Science* **285**, 599–604 (1999).
11. Tsodyks, M., Kenet, T., Grinvald, A. & Arieli, A. Linking spontaneous activity of single cortical neurons and the underlying functional architecture. *Science* **286**, 1943–1946 (1999).
12. Chiu, C. & Weliky, M. Spontaneous activity in developing ferret visual cortex in vivo. *J. Neurosci.* **21**, 8906–8914 (2001).
13. Kenet, T., Bibitchkov, D., Tsodyks, M., Grinvald, A. & Arieli, A. Spontaneously emerging cortical representations of visual attributes. *Nature* **425**, 954–956 (2003).
14. Gao, W., Newman, D. E., Wormington, A. B. & Pallas, S. Development of inhibitory circuitry in visual and auditory cortex of postnatal ferrets: Immunocytochemical localization of GABAergic neurons. *J. Comp. Neurol.* **409**, 261–273 (1999).
15. Anderson, J., Lampl, I., Reichova, I., Carandini, M. & Ferster, D. Stimulus dependence of two-state fluctuations of membrane potential in cat visual cortex. *Nature Neurosci.* **3**, 617–621 (2000).
16. Cossart, R., Aronov, D. & Yuste, R. Attractor dynamics of network UP states in the neocortex. *Nature* **423**, 283–288 (2003).
17. Shu, Y. S., Hasenstaub, A., Badoual, M., Bal, T. & McCormick, D. A. Barrages of synaptic activity control the gain and sensitivity of cortical neurons. *J. Neurosci.* **23**, 10388–10401 (2003).
18. Gallant, J. L., Connor, C. E. & Van Essen, D. C. Neural activity in areas V1, V2 and V4 during free viewing of natural scenes compared to controlled viewing. *Neuroreport* **9**, 1673–1678 (1998).
19. Vinje, W. E. & Gallant, J. L. Sparse coding and decorrelation in primary visual cortex during natural vision. *Science* **287**, 1273–1276 (2000).
20. Gawne, T. J. & Richmond, B. J. How independent are the messages carried by adjacent inferior temporal neurons? *J. Neurosci.* **13**, 2758–2771 (1993).
21. Pola, G., Thiele, A., Hoffmann, K. P. & Panzeri, S. An exact method to quantify the information transmitted by different mechanisms of correlational coding. *Network Comput. Neural Syst.* **14**, 35–60 (2003).
22. Nirenberg, S. & Latham, P. E. Decoding neuronal spike trains: How important are correlations? *Proc Natl Acad. Sci. USA* **100**, 1045–1050 (2003).
23. Kara, P., Reinagel, P. & Reid, R. C. Low response variability in simultaneously recorded retinal, thalamic, and cortical neurons. *Neuron* **27**, 635–646 (2000).
24. Hirsch, J. A. et al. Synaptic physiology of the flow of information in the cat's visual cortex in vivo. *J. Physiol. (Lond.)* **540**, 335–350 (2002).
25. Attwell, D. & Laughlin, S. B. An energy budget for signaling in the grey matter of the brain. *J. Cereb. Blood Flow Metab.* **21**, 1133–1145 (2001).
26. Lennie, P. The cost of cortical computation. *Curr. Biol.* **13**, 493–497 (2003).
27. Weliky, M., Fiser, J., Hunt, R. H. & Wagner, D. N. Coding of natural scenes in primary visual cortex. *Neuron* **37**, 703–718 (2003).

A transmembrane protein required for acetylcholine receptor clustering in *Caenorhabditis elegans*

Christelle Gally[1], **Stefan Eimer**[1], **Janet E. Richmond**[2] & **Jean-Louis Bessereau**[1]

[1]INSERM U.497, École Normale Supérieure, 46 rue d'Ulm, 75005 Paris, France
[2]University of Illinois at Chicago, Chicago, Illinois 60607, USA

....

Clustering neurotransmitter receptors at the synapse is crucial for efficient neurotransmission. Here we identify a *Caenorhabditis elegans* locus, *lev-10*, required for postsynaptic aggregation of ionotropic acetylcholine receptors (AChRs). *lev-10* mutants were identified on the basis of weak resistance to the anthelminthic drug levamisole, a nematode-specific cholinergic agonist that activates AChRs present at neuromuscular junctions (NMJs) resulting in muscle hypercontraction and death at high concentrations[1–3]. In *lev-10* mutants, the density of levamisole-sensitive AChRs at NMJs is markedly reduced, yet the number of functional AChRs present at the muscle cell surface remains unchanged. LEV-10 is a transmembrane protein localized to cholinergic NMJs and required in body-wall muscles for AChR clustering. We also show that the LEV-10 extracellular region, containing five predicted CUB domains and one LDLa domain, is sufficient to rescue AChR aggregation in *lev-10* mutants. This suggests a mechanism for AChR clustering that relies on extracellular protein–protein interactions. Such a mechanism is likely to be evolutionarily conserved because CUB/LDL transmembrane proteins similar to LEV-10, but lacking any assigned function, are expressed in the mammalian nervous system and might be used to cluster ionotropic receptors in vertebrates.

Genetic screens for *C. elegans* mutants that exhibit strong resistance to levamisole have identified four genes encoding AChR subunits and two genes that are required for the biosynthesis of levamisole-sensitive AChRs[1–3]. However, no genes required for AChR clustering were cloned despite the large size of these screens. We hypothesized that impairing the function of such genes would generate subtle phenotypes for two reasons. First, unclustered levamisole-sensitive AChRs might remain functional if properly inserted into the plasma membrane, thus conferring levamisole-sensitivity. Second, there is an additional class of AChRs present at *C. elegans* NMJs that are activated by acetylcholine and nicotine but are insensitive to levamisole[4]. These receptors, of as yet unknown composition, might compensate for a decrease in levamisole-sensitive AChRs at the synapse.

We therefore performed a screen to isolate mutants that exhibited only weak resistance to levamisole. To facilitate the identification of mutated genes we used an insertional mutagenesis based on germline mobilization of the *Drosophila* transposon *Mos1* (ref. 5). We isolated a mutant allele, *kr26*, that resulted from a *Mos1* insertion whose interpolated genetic position was in the vicinity of the *lev-10* locus. A single mutant allele of *lev-10*, *x17*, was isolated previously in a levamisole-resistance screen but was not characterized at the molecular level[1]. Using a genetic complementation test, we showed that *x17* and *kr26* are two alleles of the same gene, *lev-10*. Both *lev-10* mutants displayed a slight resistance to levamisole, when assayed by dose–response (Fig. 1a), but after 1 h of exposure to 1 mM levamisole, 100% of the *lev-10* mutants became paralysed. Although, in contrast to wild-type animals, *lev-10* mutants were able to survive while remaining hypercontracted at this elevated drug concentration. In addition, both *lev-10* mutants displayed marginal locomotory defects on plates. When movement was analysed in liquid medium, a subtle but significant movement impairment was